2026 IEEE International Conference on Robotics and Automation (ICRA 2026)
June 1-5, 2026. Vienna, Austria

Precise and Efficient Collision Prediction under Uncertainty in Autonomous Driving

Marc Kaufeld[1], Johannes Betz[1]

***Abstract*— This research introduces two efficient methods to estimate the collision risk of planned trajectories in autonomous driving under uncertain driving conditions. Deterministic collision checks of planned trajectories are often inaccurate or overly conservative, as noisy perception, localization errors, and uncertain predictions of other traffic participants introduce significant uncertainty into the planning process. This paper presents two semi-analytic methods to compute the collision probability of planned trajectories with arbitrary convex obstacles. The first approach evaluates the probability of spatial overlap between an autonomous vehicle and surrounding obstacles, while the second estimates the collision probability based on stochastic boundary crossings. Both formulations incorporate full state uncertainties, including position, orientation and velocity, and achieve high accuracy at computational costs suitable for real-time planning. Simulation studies verify that the proposed methods closely match Monte Carlo results while providing significant runtime advantages, enabling their use in risk-aware trajectory planning. The collision estimation methods are available as open-source software: `https://github.com/TUM-AVS/Collision-Probability-Estimation`**

***Index Terms*— Autonomous vehicles, trajectory planning, collision probability, risk estimation.**

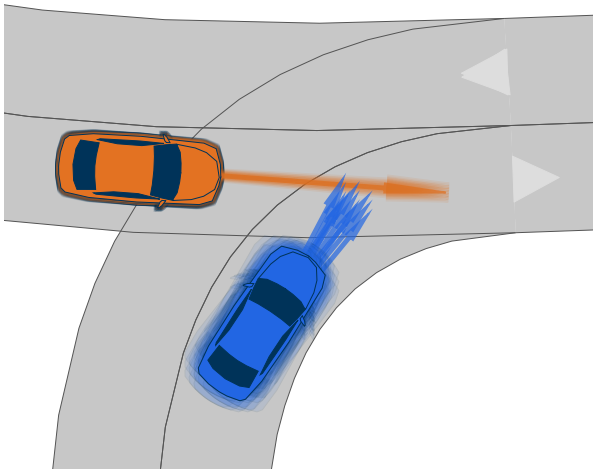

Fig. 1. Exemplary scenario with large state uncertainties for the obstacle vehicle (blue) and small ones for the AV (orange), illustrating the necessity of a probabilistic collision risk measure in motion planning.

I. Introduction

In autonomous driving, continuous collision checking is necessary for safe and collision-free motion planning [1]. In each planning cycle, planned trajectories must be checked against potential future collisions with surrounding obstacles [2]. Therefore, the autonomous vehicle (AV) needs to carefully perceive, track, and predict the behavior of nearby vehicles. However, the accuracy of the environment model and own state estimation is limited by noisy and incomplete sensor data and localization errors. Furthermore, predicting the future behavior of other traffic participants remains difficult. These uncertainties propagate into the planning process, such that deterministic collision checks, e.g., based on hierarchical bounding volumes [3], [4] are not reasonably applicable for online motion planning in autonomous driving.

Therefore, planning and control strategies must assess the likelihood of collisions, while accounting for the prevailing uncertainties to minimize both the risk to the safety of surrounding traffic and the AV's own reliable operation [5] [6]. A principled approach to achieving collision awareness entails incorporating risk metrics into decision-making, allowing the planner to explicitly trade off safety against performance. One potential strategy is to calculate the collision probability along a trajectory as the probability of spatial overlap at each time step [7]. Alternatively, the likelihood of colliding with an obstacle's boundary over a certain period of time can be determined [8].

This paper presents two methods to efficiently and accurately estimate the expected collision risk of planned trajectories for an AV under uncertain conditions. We propose two semi-analytic strategies to assess the collision probability based on probabilistic predictions of surrounding obstacles, incorporating full state uncertainties. Our findings indicate that both methods are capable of correctly forecasting the collision probability under appealing computation times.

II. Related Work

In the context of autonomous driving, two paradigms for addressing the risk of collisions along trajectories can be identified [9]: Worst-case approaches are designed to prevent the most severe safety violations, thereby ensuring a high level of safety. However, these approaches often result in overly conservative, impractical driving behaviors. Such formulations are often derived from bounding volumes, including spheres [10], ellipsoids [11], and oriented bounding boxes [12]. Additional safety margins around the obstacles account for measurement errors [4], [13]. Subsequently, reachability analysis is performed to obtain collision-free driving corridors [14]–[17]. However, in the worst case, the AV is subject to the freezing robot problem, which occurs when no collision-free driving corridor can be identified [18].

[1]M. Kaufeld and J. Betz are with the Professorship of Autonomous Vehicle Systems, TUM School of Engineering and Design, Technical University of Munich, 85748 Garching, Germany; Munich Institute of Robotics and Machine Intelligence (MIRMI), Contact: {marc.kaufeld, johannes.betz}@tum.de

Conversely, risk-aware techniques explicitly account for the distribution of possible outcomes, aiming to balance efficiency and safety. The objective of risk-aware planning is to enable autonomous vehicles to interact safely and intelligently with their environment while allowing a certain level of risk. In many cases, the evaluation of planned trajectories is conducted by means of criticality measures, including time-to-collision (TTC) or proportion of stopping distance (PSD) [19], [20]. However, these metrics assume a deterministic and simplified one-dimensional collision problem. As such, their results may differ significantly from the real values due to ignored uncertainties, leading to unexpected collisions [21].

Other authors propose barrier functions centered around the midpoint of obstacles to incorporate risk awareness. They calculate a distance-dependent risk value, but neglect the shape of the obstacle [9], [22]. These barrier functions can incorporate positional uncertainties by defining a probability-dependent threshold value, but remain an estimated value [23], [24].

An alternative approach involves calculating the probability of collision as the percentage of spatial overlap between the ego vehicle and an obstacle, whose position is assumed to be uncertain and can be described by a probability density function (PDF). The collision probability is then incorporated into motion planning as a risk constraint [25], [26]. Typically, the ego vehicle's position and the relative orientation between the ego and obstacles are assumed to be deterministic. The percentage of spatial overlap can generally be obtained by means of Monte Carlo sampling [7], [27]. However, this method is computationally expensive and therefore not applicable in real-time for autonomous driving [21]. Consequently, the calculation of collision probability must be performed in a more efficient manner, for instance, by integrating the positional PDF over the collision domain. However, for arbitrarily shaped objects, these integrals often lack analytic solutions. Some authors have thus proposed simplifications, such as the use of robots approximated as points [28], [29], (multiple) spheres [30]–[32], or rectangles with deterministic orientation [33].

All previously presented approaches are derived under the assumption of statistical independence between states of an obstacle at different time steps. However, since this assumption does not hold for predicted trajectories, the collision probability of planned trajectories cannot be accumulated over time as a total collision risk [34]. Consequently, a common approach for evaluating the collision probability along a trajectory or a certain time horizon is to use the maximum risk value over that period [19], [35]. Alternatively, a survival probability is proposed in [22], that uses the spatial overlap and utilizes a truncation approximation to model the temporal dependency of the collision risk. The authors of [8] derive an alternative approach centered on the calculation of boundary crossing probabilities in stochastic vector processes. However, their method does not account for orientation distributions or moving ego vehicles, and it provides only an approximate solution.

A. Contributions

In this paper, we address the precise prediction of the collision risk for future trajectories to enable AVs to plan efficiently and safely in a risk-aware manner under uncertain conditions.

- We derive two exact mathematical formulations to calculate the collision probability between arbitrary convex-shaped obstacles.
- Both methods are capable of coping with uncertain conditions prevalent in the AV software stack by incorporating uncertainties about the pose, orientation, and velocity of surrounding obstacles.
- Our approaches demonstrate compelling computational performance, making them applicable to time-limited computing applications in autonomous vehicles.

III. Methodology

In this section, we state both semi-analytic formulations for calculating the collision probability. First, we derive a method based on spatial overlap in section III-A. Subsequently, we introduce an alternative formulation based on the probability of boundary crossings in section III-B. We consider the general motion planning problem for an AV operating in dynamic traffic environments. At each time step t, the planner generates a candidate trajectory $\zeta_i(t) = \{(\mathbf{x}_e^\tau, \mathbf{v}_e^\tau), \tau \in [t, t+T]\}$ over a finite planning horizon T. The trajectory is represented as a sequence of states $\mathbf{x}_e^\tau = (x_e^\tau, y_e^\tau, \theta_e^\tau)$ and velocities $\mathbf{v}_e^\tau = (v_{x,e}^\tau, v_{y,e}^\tau)$, where the states comprise the position of the vehicle center (x_e^τ, y_e^τ) and the vehicle heading θ_e^τ. In practice, a motion planner evaluates candidate trajectories according to a cost functional that typically balances smoothness, progress, and safety. The optimal trajectory is then executed for a short time increment Δt before replanning in a receding horizon fashion [36]. The collision probability derived below serves as a quantitative safety metric for evaluating the risk of a planned trajectory. To assess the likelihood of a collision along a specific trajectory, the future motion of surrounding traffic participants must be predicted. We assume that a probabilistic prediction of surrounding vehicles is available, e.g., through a preceding prediction module. Due to perception noise, state estimation errors, and the inherent uncertainty in forecasting the behavior of traffic participants, the predicted states and velocities of obstacles are subject to aleatoric and epistemic uncertainty. Accordingly, we model the predicted states and velocities of each obstacle by a time-dependent PDF $p_o(\tau) = p(\mathbf{x}_o^\tau, \mathbf{v}_e^\tau)$. Similarly, the ego vehicle trajectory may be subject to uncertainty due to localization errors that are potentially not negligible, sensor noise, as well as process disturbances $p_e(\tau) = p(\mathbf{x}_e^\tau, \mathbf{v}_e^\tau)$. While state and velocity uncertainties within a single agent may be correlated, we assume independence between the ego vehicle and obstacle distributions. This is to say, p_e and p_o are statistically independent because ego uncertainty mainly stems from localization and process noise, whereas obstacle uncertainty arises from perception errors and behavioral prediction uncertainty.

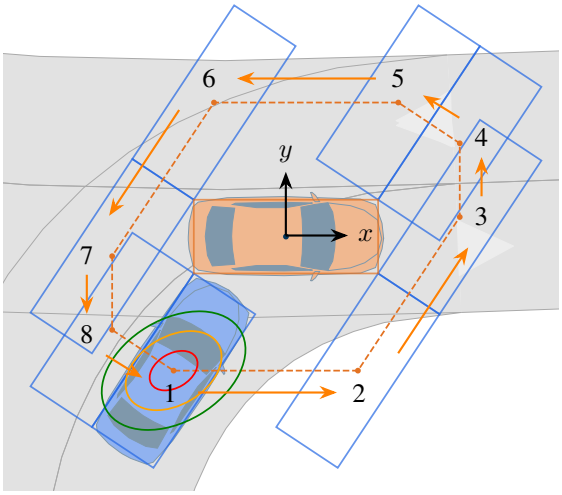

Fig. 2. Combined collision volume of the ego AV (orange) and an obstacle vehicle (blue). Vehicles are approximated as rectangles. The ellipses over the blue vehicle illustrate the combined positional covariance $\mathbf{\Sigma_x}$

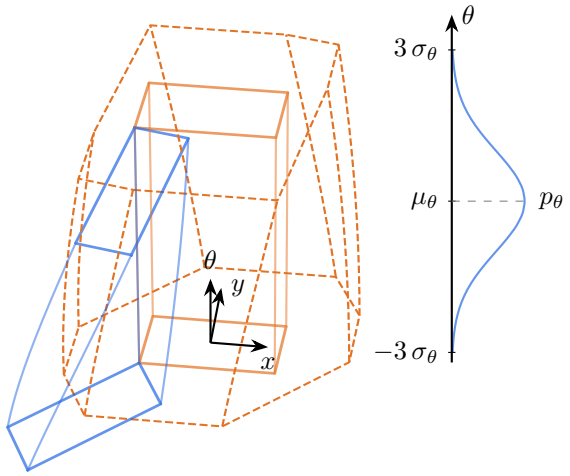

Fig. 3. The orientation-dependent collision polyhedron. It is the same scenario as in fig. 2 but with an orientation variance of $\sigma_\theta^2 = 0.01\,\mathrm{rad}^2$. The third dimension illustrates the change in the shape of the collision volume. The distribution on the right indicates the PDF of the relative orientation θ.

A. Probability of Spatial Overlap

As the following calculations are valid for all time steps, the time index τ will be omitted in the following chapter to enhance readability. The probability of a collision at any given time step can be interpreted as the probability of spatial overlap, given that a collision is defined as the intersection of the ego's occupancy and that of an external obstacle [8]. After marginalizing out the velocity components, the pose distributions of the ego and obstacle are obtained as

$$p_{\mathbf{x}_j} = \int p_j \, d\mathbf{v}, \quad j \in \{o, e\}. \tag{1}$$

The probability of spatial overlap can then be expressed as an integral over the joint pose distributions,

$$P_c = \iint I_c(\mathbf{x}_e, \mathbf{x}_o) p_{\mathbf{x}_e} p_{\mathbf{x}_o} \, d\mathbf{x}_o \, d\mathbf{x}_e, \tag{2}$$

where the indicator function I_c describes whether the occupied regions intersect,

$$I_c(\mathbf{x}_e, \mathbf{x}_o) = \begin{cases} 1 & \texttt{Occ}(\mathbf{x}_e) \cap \texttt{Occ}(\mathbf{x}_o) \neq \emptyset \\ 0 & \text{else.} \end{cases} \tag{3}$$

Because the indicator function introduces a discontinuity, a direct analytic solution of eq. (2) is, in most cases, not possible. A more tractable formulation is obtained by considering the relative pose between the ego vehicle and an obstacle $\mathbf{x} = \mathbf{x}_o - \mathbf{x}_e$. The probability density of $\mathbf{x}$ follows from convolving the two marginal pose densities, $p_\mathbf{x} = p_{\mathbf{x}_e} * p_{\mathbf{x}_o}$. In the event that both uncertainties are modeled as multivariate normal distributions $p_i \sim \mathcal{N}(\mu_i, \mathbf{\Sigma}_i)$, $i \in \{\mathbf{x}_o, \mathbf{x}_e\}$, the convolution has a closed-form solution, which is again Gaussian,

$$\begin{aligned} p_\mathbf{x} \sim & \mathcal{N}(\mu_\mathbf{x}, \mathbf{\Sigma_x}) \\ & \text{with} \\ & \mu_\mathbf{x} = \mu_{\mathbf{x}_o} - \mu_{\mathbf{x}_e}, \quad \mathbf{\Sigma_x} = \mathbf{\Sigma}_{\mathbf{x}_o} + \mathbf{\Sigma}_{\mathbf{x}_e}. \end{aligned} \tag{4}$$

Substituting the relative formulation, eq. (2) reduces to integrating $p_\mathbf{x}$ over a combined collision volume Ω,

$$P_c = \iiint_\Omega p_\mathbf{x}(x, y, \theta) \, dx \, dy \, d\theta. \tag{5}$$

The resulting value corresponds to the probability that the obstacle's center lies within the collision volume spanned around the ego vehicle. When the orientational variance is neglected, the collision volume is defined by the Minkowski sum of the shapes of the colliding obstacles $\Omega = S_e \oplus S_o$. In a birds-eye view representation, this is equivalent to the trace of the obstacle center swept around the hull of the ego vehicle as illustrated in fig. 2. For any combination of two convex polygons, the collision volume is again a convex polygon, and it can be efficiently calculated by merging the edges based on their orientation with respect to the origin [37]. For collision checking in autonomous driving, where road users such as vehicles or bicycles are often approximated as rectangles, the calculation of the Minkowski sum simplifies to the sum of the oriented and signed half-lengths and -widths of one shape with respect to the other.

If the relative orientation between the ego AV and the obstacle is not deterministic, the collision volume is not fixed, but depends on the marginal orientation distribution, $\Omega = \Omega(p_\theta)$, resulting in a polyhedron as shown in fig. 3. With conditioning on the orientation, integral (5) can be rewritten as

$$P_c = \int_\theta \Big(\int_{y(\theta)} \int_{x(\theta)} p_\mathbf{x}(x, y \mid \theta) \, dx \, dy \Big) p_\theta \, d\theta. \tag{6}$$

Thus far, no assumptions have been made about the shape of the distribution. Since they might have correlated components and could be elongated, e.g., through rotated anisotropic distributions, we perform Cholesky whitening [38] to transform the relative pose and the collision

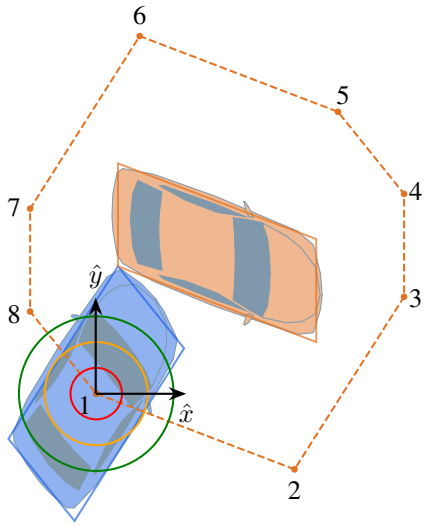

Fig. 4. The collision volume from the scenario illustrated in fig. 2 after whitening transformation.

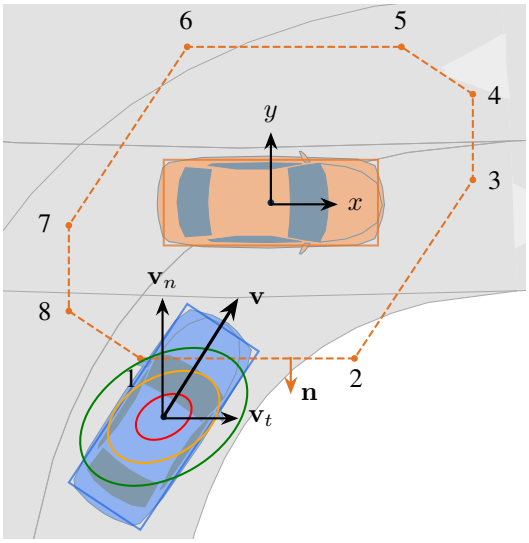

Fig. 5. Illustration of the normal velocity for the boundary crossing rate along the segment $1-2$ of the collision volume.

volume to be isotropic and centered around the midpoint of the obstacle,

$$\hat{\mathbf{x}} = \mathbf{W}_{\mathbf{x}}(\mathbf{x} - \mu_{\mathbf{x}}), \tag{7}$$

$$\hat{\mathbf{\Sigma}}_{\mathbf{x}} = \mathbf{W}_{\mathbf{x}}\mathbf{\Sigma}_{\mathbf{x}}{\mathbf{W}_{\mathbf{x}}}^T = \mathbf{I}. \tag{8}$$

$\mathbf{W}$ is a transformation matrix such that ${\mathbf{W}_{\mathbf{x}}}^T\mathbf{W}_{\mathbf{x}} = \mathbf{\Sigma}^{-1}$ and can, for example, be obtained by Cholesky decomposition of the inverse covariance ${\mathbf{\Sigma}_{\mathbf{x}}}^{-1} = \mathbf{L}\mathbf{L}^T$ as $\mathbf{W} = \mathbf{L}^T$. By whitening, all directions become independent and share the same uniform variance $\mu_i = 0, \sigma_i = 1,\ i \in \{\hat{x}, \hat{y}, \hat{\theta}\}$ (compare fig. 4), making the solution procedure numerically more stable and efficient without altering the final result. For a fixed θ and a convex and whitened collision volume with N sides, the inner integral in eq. (6) can now be written as

$$P_c(\hat{\mathbf{x}} \mid \hat{\theta}) = \sum_{n=1}^{N} \int_{\hat{x}=x_{l,n}(\hat{\theta})}^{x_{h,n}(\hat{\theta})} p_{\hat{x}}(\hat{x}) \Big(\int_{\hat{y}=0}^{y_{h,n}(\hat{x},\hat{\theta})} p_{\hat{y}}(\hat{y})\, d\hat{y} \Big)\, d\hat{x}, \tag{9}$$

where the sequential integration limits $x_{l,n}, x_{h,n}$ are the $\hat{x}$-coordinates of the N corners of the collision volume at a given relative orientation $\hat{\theta}$ in anti-clockwise direction and $\hat{y}_{h,n}$ is defined by their connecting line $\hat{y}_{h,n}(\hat{x}, \hat{\theta}) = m_n(\hat{\theta})\hat{x} + b_n(\hat{\theta})$. Evaluating the inner integral, the formulation reduces to one dimension,

$$P_c(\hat{\mathbf{x}} \mid \hat{\theta}) = \sum_{n=1}^{N} \int_{\hat{x}=x_{l,n}(\hat{\theta})}^{x_{h,n}(\hat{\theta})} p_{\hat{x}}(\hat{x}) \Big(F_{\hat{y}}(y_{h,n}) - F_{\hat{y}}(0) \Big)\, d\hat{x}, \tag{10}$$

with $F_{\hat{y}}$ being the cumulative distribution function of $p_{\hat{y}}$. This expression can be solved numerically very efficiently. Assuming a multivariate Gaussian distribution, the probability of spatial overlap for one time step becomes

$$P_c(\hat{\mathbf{x}} \mid \hat{\theta}) = \sum_{n=1}^{N} \frac{1}{\sqrt{8\pi}} \int_{\hat{x}=x_{l,n}(\hat{\theta})}^{x_{h,n}(\hat{\theta})} \exp\!\left(\frac{-\hat{x}^2}{2}\right) \operatorname{erf}\!\left(\frac{y_{h,n}}{\sqrt{2}}\right) d\hat{x}, \tag{11}$$

with

$$y_{h,n} = m_n(\hat{\theta})\hat{x} + b_n(\hat{\theta}).$$

For additional consideration of the orientation uncertainty, one now needs to solve the outer integral in eq. (6),

$$P_c = \int_{\hat{\theta}} p_{\hat{\theta}}(\hat{\theta}) P_c(\hat{\mathbf{x}} \mid \hat{\theta})\, d\hat{\theta}, \tag{12}$$

which again can be solved effectively by numerical integration. This expression yields the probability of partial overlap at a given time step under position and orientation uncertainties. To evaluate the collision risk along a trajectory, one can either take the maximum value $P_c = \max_{\tau \in T}\{P_c^\tau\}$, or, if temporal independence of the states is assumed, the total collision probability over a trajectory with a planning horizon of T is

$$P_c = 1 - \prod_{\tau=0}^{T} (1 - P_c^\tau). \tag{13}$$

B. Boundary Crossing Probability

In the preceding chapter, we presented a methodology for calculating the probability of collision between an ego AV and an obstacle by estimating the spatial overlap between them. However, real-world collisions are better characterized by vehicles impacting each other, resulting in the structural intrusion of the chassis of the other vehicles from the front, rear, or sides. In order to accurately reflect this behavior, we present a formulation for the calculation of the collision probability based on stochastic boundary crossing processes,

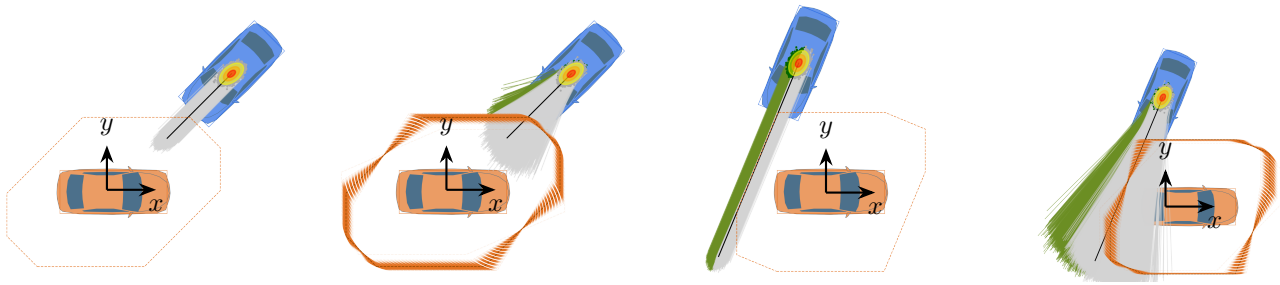

(a) Scenario 1 without orientation uncertainty: Obstacle vehicle approaches the ego AV from the front left

(b) Scenario 1 with orientation uncertainty: The different collision boundaries indicate the uncertainties in the relative orientation

(c) Scenario 2 without orientation uncertainty: Obstacle vehicle approaches the ego AV with offset from the side

(d) Scenario 2 with orientation uncertainty: The different collision boundaries indicate the uncertainties in the relative orientation

Fig. 6. Considered collision scenarios. The drawn trajectories are sampled using a constant velocity model and an Extended Kalman Filter. Gray ones collide, while the green ones are collision-free. The black trajectory denotes the mean. The ellipses over the obstacle vehicle illustrate the positional variance.

as proposed in [8]. The number of boundary crossings of a particle within a given time interval is equivalent to the integration of the boundary crossing rate over this interval. Analogously, the probability of boundary crossings is defined as the time integral over the crossing probability rate $\dot{P}_{bc}$,

$$P_c = \int_{\tau=t}^{T} \dot{P}_{bc}\, d\tau. \tag{14}$$

For collision checking, the probability rate of boundary crossings is derived in detail in [8]. With a state and velocity distribution $p(\mathbf{x}, \mathbf{v})$ at the center point of an obstacle, the collision probability rate is defined as the expected velocity pointing into the collision volume, while the center is located at the boundary of the collision volume,

$$\dot{P}_{bc} = -\iint\limits_{\substack{\mathbf{x}\in\partial\Omega,\\ v_n\leq 0}} v_n p(\mathbf{x}, \mathbf{v})\, d\mathbf{x}\, d\mathbf{v}. \tag{15}$$

The value $v_n = \mathbf{n}^T(\mathbf{x})\mathbf{v}$ denotes the velocity component normal to the volume boundary $\partial\Omega$. By making use of the conditional distribution of the velocity and after marginalizing the tangential velocity, we can rewrite eq. (15) as

$$\begin{aligned}\dot{P}_{bc} &= -\int_{\mathbf{x}\in\partial\Omega} \left(\int_{v_n\leq 0} v_n p(v_n \mid \mathbf{x})\, dv_n \right) p_{\mathbf{x}}(\mathbf{x})\, d\mathbf{x} \\ &= \int_{\mathbf{x}\in\partial\Omega} \left(\mathbb{E}\left[v_n^- \mid \mathbf{x}\right] \right) p_{\mathbf{x}}(\mathbf{x})\, d\mathbf{x}.\end{aligned} \tag{16}$$

The inner integral thereby yields the expected inward normal velocity along the boundary and is given by the truncated mean of the distribution cropped at $v_n = 0$, which for a Gaussian has an analytic solution,

$$\begin{aligned}\mathbb{E}\left[v_n^- \mid \mathbf{x}\right] &= -\mu_{v_n|\mathbf{x}}\, F\big(-z\big) + \sigma_{v_n|\mathbf{x}}\, p\big(z\big), \\ &\text{with} \\ z &= \frac{\mu_{v_n|\mathbf{x}}}{\sigma_{v_n|\mathbf{x}}}, \\ \mu_{v_n|\mathbf{x}} &= \mathbf{n}^T\big(\mu_v + \boldsymbol{\Sigma}_{vx}\boldsymbol{\Sigma}_x^{-1}(\mathbf{x} - \mu_{\mathbf{x}})\big), \\ \sigma^2_{v_n|\mathbf{x}} &= \mathbf{n}^T\big(\boldsymbol{\Sigma}_v - \boldsymbol{\Sigma}_{vx}\boldsymbol{\Sigma}_x^{-1}\boldsymbol{\Sigma}_{xv}\big)\mathbf{n}.\end{aligned} \tag{17}$$

As for the overlap probability, we can decompose the polygonal collision volume into N linear edges, parametrized as $\mathbf{x}_n(s) = (1-s)\mathbf{x}_{l,i} + s\mathbf{x}_{h,i}$. We can thus rewrite the boundary integral as the sum of one-dimensional integrals along the edges,

$$\dot{P}_{bc} = -\sum_{i=1}^{N} \int_{s=0}^{1} \mathbb{E}\left[v_n^- \mid \mathbf{x}_i(s)\right] p\big(\mathbf{x}_i(s)\big)\, \ell_i ds, \tag{18}$$

with the edge length ℓ_i as the Jacobian for the variable change. This expression can again be efficiently solved using numerical integration schemes. For the boundary crossing rate, the distributions do not benefit from whitening, since it relies on evaluating 1D line integrals rather than volume integrals used in the spatial overlap calculation, and is therefore not performed in this method. For the integration of orientation uncertainties, one can proceed as in section III-A and first condition the probability rate on the orientation $\dot{P}_{bc}(\mathbf{x} \mid \theta)$, followed by an integration along the third dimension of the orientation-dependent polyhedron.

IV. Experiments & Results

In this section, we first demonstrate the functionality of the proposed methods using Monte Carlo simulation, followed by an application study as trajectory evaluation in a sampling-based motion planner. Numerical integrations are done with Gauss-Legendre quadrature with 51 interpolation points.

A. Comparison with Monte Carlo Sampling

We consider two scenarios with a prediction horizon of $T = 3\,\mathrm{s}$ each, once with orientation uncertainty and once without (see fig. 6). In the first scenario, the obstacle vehicle approaches the ego AV from the front left at a constant velocity, resulting in a collision probability of nearly $100\,\%$. In the second scenario, the other vehicle approaches the ego AV with a slight offset from the side at higher velocities. This scenario results in a collision probability of approximately $60\,\%$. The exact simulation data are shown in Table I.

We first evaluate the collision probability using five different approaches. To evaluate the spatial overlap probability,

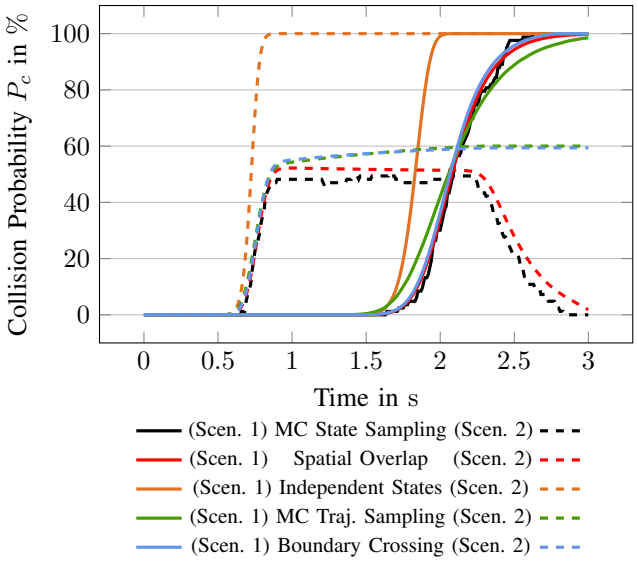

Fig. 7. Collision probability without orientation uncertainties

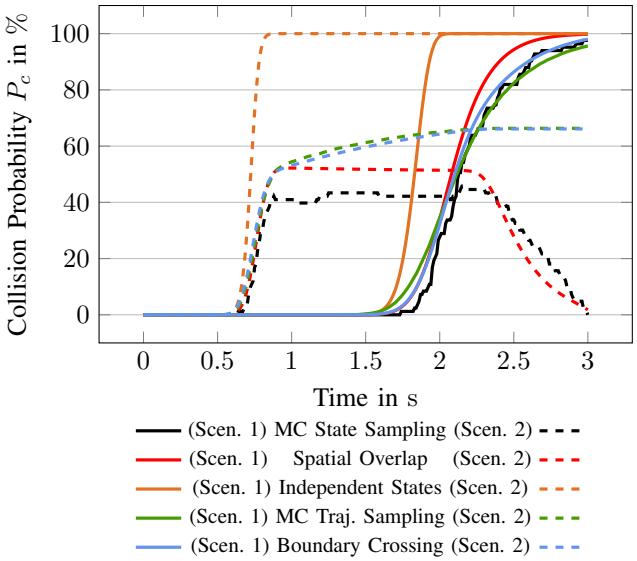

Fig. 8. Collision probability with orientation uncertainties

TABLE I

INITIAL MEAN AND VARIANCE OF THE SIMULATED EGO AND OBSTACLES, EACH IN THE GLOBAL COORDINATE SYSTEM.

Value	Ego AV	Obs. scenario 1	Obs. scenario 2
$\mu_{\mathbf{x}}^0$ in m	$(0, 0)$	$(5.5, 5.5)$	$(-1.5, 6)$
$\Sigma_{\mathbf{x}}^0$ in m^2	$\begin{bmatrix} 0.1^2 & 0 \\ 0 & 0.05^2 \end{bmatrix}$	$\begin{bmatrix} 0.2^2 & 0 \\ 0 & 0.1^2 \end{bmatrix}$	$\begin{bmatrix} 0.2^2 & 0 \\ 0 & 0.1^2 \end{bmatrix}$
μ_v^0 in m s^{-1}	0	1.4	3.25
σ_v^0 in m s^{-1}	0.1	0.1	0.1
θ^0 in rad	0	$-\pi/4$	$-3\pi/8$
σ_θ^0 in rad	0/0.1	0/0.1	0/0.1

we perform Monte Carlo sampling for each state along the predicted trajectory independently and calculate the proportion of collided samples per timestep (MC State Sampling). Second, we calculate the probability of spatial overlap at each time step using eq. (12), and third, we evaluate the collision probability under the assumption of temporal independence, as described by eq. (13). To compare the probability of boundary penetrations (eq. (14)), we sample complete trajectories using Monte Carlo (MC Traj. Sampling). A trajectory contributes to the collision probability only after the collision time step. In both sampling-based methods, we sample 25000 states and trajectories, respectively. In fig. 7, the resulting collision probabilities are plotted over time for both scenarios when the orientation uncertainties are neglected. For the colliding scenario (scenario 1), all approaches predict a collision probability of 1. However, it can be observed that the assumption of independent states does not reflect reality, leading to an excessively conservative collision probability, which is more than 0.5 s earlier at 100 % than the other methods. All other approaches yield similar results with an increasing collision probability between 1.5 s and 2.5 s. Only the trajectory sampling approach stands out to some extent as it ascends earlier, but with a slightly lower slope. In the second scenario in fig. 7, where a collision probability of approximately 60 % can be observed, the independence assumption again significantly overestimates the collision risk. Spatial overlap yields a maximum collision probability of 53 % after ca. 0.8 s and then decreases towards the end of the time period, when the obstacle vehicle has already passed the rear of the ego AV. The tendency matches state sampling but predicts a minimal increase in the maximum collision probability. In contrast, the boundary crossing probability initially rises similarly to the overlap probability, but continues to increase as the obstacle vehicle drives along the collision volume. It correctly matches the collision probability of the trajectory sampling approach and thus captures the temporal dependencies arising from the probabilistic normal velocity along the boundary.

In fig. 8, the collision probabilities for the scenarios including orientation uncertainties are illustrated. The overall tendencies are identical to the first case. The spatial overlap calculation again overestimates the probability by approximately 10 % in the second scenario, whereas the boundary crossing probability aligns well with the collision probabilities of the sampled trajectories. However, when including the orientation in the analysis, the overall collision probability in the second scenario increases from 60 % to 66 %, highlighting the necessity to include orientation deviations in the collision analysis, since small changes in the initial orientation of predictions can result in significantly different collision probabilities.

Next, we compare the runtime of our proposed methods. For trajectory evaluation in motion planning for autonomous driving, it is important to achieve fast calculation times. In table II, we list the mean computation times on a 12th Gen Intel Core i7 processor. Both proposed methods are significantly faster than the sampling-based approaches. The computation times for our overlap probability implementation are lower

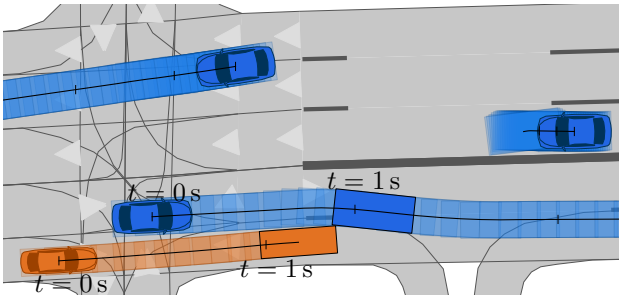

(a) Planning without residual risk. Potentially colliding trajectories are filtered out, resulting in an end of the simulation after $1.2\,\mathrm{s}$ since no collision-free trajectories are found.

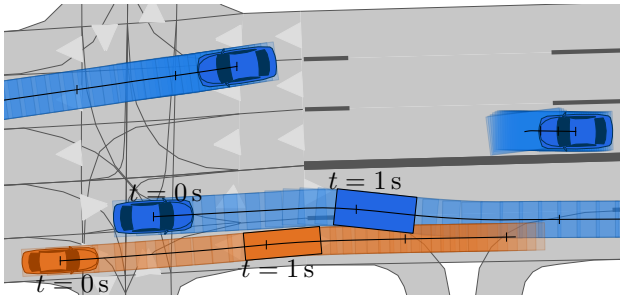

(b) Planning with probability based collision estimation. The Planner can select trajectories with residual risk.

Fig. 9. Simulated cut-in scenario. The ego AV is the orange vehicle, while all blue ones are controlled by the simulation. The occupancies show the final trajectories. The highlighted occupancy illustrates in both images the final time step of the conservative approach after $1.2\,\mathrm{s}$.

than those for the boundary crossing rate. However, both remain below $0.1\,\mathrm{s}$ and $0.01\,\mathrm{s}$ with and without orientation, respectively.

TABLE II
RUNTIME ANALYSIS OF THE COLLISION PROBABILITY ALONG THE COMPLETE TRAJECTORY IN S.

Method	Without Orientation	With Orientation
MC State Sampling	0.3	10.3
Spatial Overlap	0.001	0.02
MC Traj. Sampling	1.9	2.5
Boundary Crossing	0.003	0.09

B. Application Example in an Analytic Motion Planner

Finally, we integrate our proposed collision probability calculations into a sampling-based motion planning framework [36] and simulate a critical cut in maneuver. In each iteration, the planner evaluates 600 sampled trajectories. The predicted collision risk is thereby incorporated into the cost function to select the trajectory with the lowest risk. As a comparison, we use a conservative collision check that filters out all trajectories that intersect the oriented bounding box covering the 3σ region around the predicted obstacle location, avoiding any risk in the planning process. The uncertainties are forecasted along the obstacle trajectory using a Kalman Filter assuming a symmetric pose variance of $\sigma_x = \sigma_y = 0.3\,\mathrm{m}$ and a velocity variation of $\sigma_v = 0.15\,\mathrm{m\,s^{-1}}$. In fig. 9, we show the resulting final paths. For the situation where all collision risk is avoided (fig. 9a), the planner is only able to plan for $1.2\,\mathrm{s}$. Afterwards, it does not find any collision-free trajectory. In contrast, by allowing some residual risk, the planner is able to solve the situation by selecting a potentially riskier trajectory, which decelerates the car strongly enough to eventually avoid the rear-end collision (fig. 9b). The same results can be obtained using both proposed methods, maximum spatial overlap and boundary crossing probability.

Since our proposed collision prediction formulations can be easily vectorized, the computation time per trajectory batch remains small, with approximately $0.08\,\mathrm{s}$ for the overlap probability and $0.15\,\mathrm{s}$ for the boundary penetrations.

V. DISCUSSION

Our results demonstrate the effectiveness of both proposed methods for collision risk prediction under uncertainty. The semi-analytic formulation of the spatial overlap probability closely matches estimates obtained from Monte Carlo state sampling, while the boundary crossing formulation aligns well with collision probabilities derived from full trajectory sampling. Furthermore, the experiments proved that assuming independence of states along a trajectory leads to overly conservative and unrealistic risk estimates, since predicted states are inherently correlated over time. While the spatial overlap formulation provides an efficient collision probability metric, it does not fully capture the physical nature of real-world collisions. In motion planning, temporal dependencies must be considered when ultimately assessing the safety of planned trajectories. In this regard, the boundary crossing formulation offers a more realistic representation of collision events by explicitly modeling the stochastic inward normal velocity along the collision boundary. Although this approach incurs slightly higher computational cost, it more accurately reflects the underlying collision dynamics.

The experiments also indicate that incorporating orientational uncertainty can be critical for reliable risk estimation. Even small deviations in the predicted heading of an obstacle can noticeably increase the collision probability. We showed in an exemplary edge case scenario that the collision probability can increase significantly from $60\,\%$ to $66\,\%$. Neglecting orientation uncertainty may therefore lead to systematic underestimation of risk in certain configurations.

VI. CONCLUSION AND FUTURE OUTLOOK

This paper presents two efficient methods for the accurate prediction of the collision risk along planned trajectories for autonomous driving. Both methods consider prevailing state uncertainties arising from sensor and prediction inaccuracies. A fast estimate can be obtained by computing the probability of spatial overlap, while a more accurate method based on boundary crossing rates yields more precise

results. The findings also highlight the necessity to include obstacle orientations in the collision risk calculation, as even small deviations in the detected heading can yield significant differences in the estimated collision probability.

Future research will extend the framework beyond Gaussian assumptions to better capture real-world sensor noise and prediction errors. As the mathematical formulations are distribution-agnostic, they remain valid for other probability distributions as well. In addition, both methods will be tested under real-world driving conditions to further validate robustness and efficiency.

REFERENCES

[1] Q. Nie, Y. Zhao, L. Xu, and B. Li, "A Survey of Continuous Collision Detection," in *2020 2nd International Conference on Information Technology and Computer Application (ITCA)*. IEEE, 2020, pp. 252–257.

[2] S. Annell, A. Gratner, and L. Svensson, "Probabilistic collision estimation system for autonomous vehicles," in *2016 IEEE 19th International Conference on Intelligent Transportation Systems (ITSC)*. IEEE, 2016, pp. 473–478.

[3] P. Jiménez, F. Thomas, and C. Torras, "Collision detection algorithms for motion planning," in *Robot Motion Planning and Control*, J. P. Laumond, Ed. Springer-Verlag, 1998, vol. 229, pp. 305–343.

[4] C. Pek, V. Rusinov, S. Manzinger, M. C. Uste, and M. Althoff, "CommonRoad Drivability Checker: Simplifying the Development and Validation of Motion Planning Algorithms," in *2020 IEEE Intelligent Vehicles Symposium (IV)*. IEEE, 2020, pp. 1013–1020.

[5] W. Schwarting, J. Alonso-Mora, and D. Rus, "Planning and Decision-Making for Autonomous Vehicles," *Annu. Rev. Control Robot. Auton. Syst.*, vol. 1, pp. 187–210, 2018.

[6] R. McAllister, Y. Gal, A. Kendall, M. Van Der Wilk, A. Shah, R. Cipolla, and A. Weller, "Concrete Problems for Autonomous Vehicle Safety: Advantages of Bayesian Deep Learning," in *Proceedings of the Twenty-Sixth International Joint Conference on Artificial Intelligence*. International Joint Conferences on Artificial Intelligence Organization, 2017, pp. 4745–4753.

[7] A. Lambert, D. Gruyer, and G. Saint Pierre, "A fast Monte Carlo algorithm for collision probability estimation," in *2008 10th International Conference on Control, Automation, Robotics and Vision*. IEEE, 2008, pp. 406–411.

[8] R. Altendorfer and C. Wilkmann, "A new approach to estimate the collision probability for automotive applications," *Automatica*, vol. 127, p. 109497, 2021.

[9] P. Akella, A. Dixit, M. Ahmadi, L. Lindemann, M. P. Chapman, G. J. Pappas, A. D. Ames *et al.*, "Risk-Aware Robotics: Tail Risk Measures in Planning, Control, and Verification," *IEEE Control Syst.*, vol. 45, pp. 46–78, 2025.

[10] Q. Xiaoyan, M. Ling, and Y. Chengzhu, "Research of collision detection algorithm based on hybrid bounding box for complex environment," in *2016 International Conference on Integrated Circuits and Microsystems (ICICM)*. IEEE, 2016, pp. 248–252.

[11] Y.-K. Choi, W. Wang, Y. Liu, and M.-S. Kim, "Continuous Collision Detection for Two Moving Elliptic Disks," *IEEE Trans. Robot.*, vol. 22, pp. 213–224, 2006.

[12] S. Gottschalk, M. C. Lin, and D. Manocha, "OBBTree: A hierarchical structure for rapid interference detection," in *Proceedings of the 23rd Annual Conference on Computer Graphics and Interactive Techniques*. ACM, 1996, pp. 171–180.

[13] R. Zapata, P. Lépinay, and P. Thompson, "Reactive behaviors of fast mobile robots," *J. Robotic Syst.*, vol. 11, pp. 13–20, 1994.

[14] A. Shkolnik, M. Walter, and R. Tedrake, "Reachability-guided sampling for planning under differential constraints," in *2009 IEEE International Conference on Robotics and Automation*. IEEE, 2009, pp. 2859–2865.

[15] S. Kousik, S. Vaskov, F. Bu, M. Johnson-Roberson, and R. Vasudevan, "Bridging the gap between safety and real-time performance in receding-horizon trajectory design for mobile robots," *The International Journal of Robotics Research*, vol. 39, pp. 1419–1469, 2020.

[16] S. Manzinger, C. Pek, and M. Althoff, "Using Reachable Sets for Trajectory Planning of Automated Vehicles," *IEEE Trans. Intell. Veh.*, vol. 6, pp. 232–248, 2021.

[17] N. Kochdumper and S. Bak, "Real-Time Capable Decision Making for Autonomous Driving Using Reachable Sets," in *2024 IEEE International Conference on Robotics and Automation (ICRA)*. IEEE, 2024, pp. 14 169–14 176.

[18] P. Trautman and A. Krause, "Unfreezing the robot: Navigation in dense, interacting crowds," in *2010 IEEE/RSJ International Conference on Intelligent Robots and Systems*. IEEE, 2010, pp. 797–803.

[19] J. Jansson, *Collision Avoidance Theory with Application to Automotive Collision Mitigation*. Department of Electrical Engineering, Linköping University, 2005.

[20] L. Westhofen, C. Neurohr, T. Koopmann, M. Butz, B. Schütt, F. Utesch, B. Neurohr *et al.*, "Criticality Metrics for Automated Driving: A Review and Suitability Analysis of the State of the Art," *Arch Computat Methods Eng*, vol. 30, pp. 1–35, 2023.

[21] A. Lambert, D. Gruyer, G. S. Pierre, and A. N. Ndjeng, "Collision Probability Assessment for Speed Control," in *2008 11th International IEEE Conference on Intelligent Transportation Systems*. IEEE, 2008, pp. 1043–1048.

[22] F. Muller and J. Eggert, "Time-Course Sensitive Collision Probability Model for Risk Estimation," in *2020 IEEE 23rd International Conference on Intelligent Transportation Systems (ITSC)*. IEEE, 2020, pp. 1–8.

[23] M. Geisslinger, F. Poszler, and M. Lienkamp, "An ethical trajectory planning algorithm for autonomous vehicles," *Nat Mach Intell*, vol. 5, pp. 137–144, 2023.

[24] W. Schwarting, J. Alonso-Mora, L. Paull, S. Karaman, and D. Rus, "Safe Nonlinear Trajectory Generation for Parallel Autonomy With a Dynamic Vehicle Model," *IEEE Trans. Intell. Transport. Syst.*, vol. 19, pp. 2994–3008, 2018.

[25] T. Brudigam, M. Olbrich, D. Wollherr, and M. Leibold, "Stochastic Model Predictive Control With a Safety Guarantee for Automated Driving," *IEEE Trans. Intell. Veh.*, vol. 8, pp. 22–36, 2023.

[26] I. Batkovic, M. Ali, P. Falcone, and M. Zanon, "Safe Trajectory Tracking in Uncertain Environments," *IEEE Trans. Automat. Contr.*, pp. 1–14, 2022.

[27] N. Goulet, Q. Wang, and B. Ayalew, "Probabilistic constraint tightening techniques for trajectory planning with predictive control," *Journal of the Franklin Institute*, vol. 359, pp. 6142–6172, 2022.

[28] N. E. Du Toit and J. W. Burdick, "Probabilistic Collision Checking With Chance Constraints," *IEEE Trans. Robot.*, vol. 27, pp. 809–815, 2011.

[29] S. Patil, J. Van Den Berg, and R. Alterovitz, "Estimating probability of collision for safe motion planning under Gaussian motion and sensing uncertainty," in *2012 IEEE International Conference on Robotics and Automation*. IEEE, 2012, pp. 3238–3244.

[30] J. Park and J. Kim, "Predictive Evaluation of Ship Collision Risk Using the Concept of Probability Flow," *IEEE J. Oceanic Eng.*, vol. 42, pp. 836–845, 2017.

[31] C. Park, J. S. Park, and D. Manocha, "Fast and Bounded Probabilistic Collision Detection for High-DOF Trajectory Planning in Dynamic Environments," *IEEE Trans. Automat. Sci. Eng.*, vol. 15, pp. 980–991, 2018.

[32] L. Tolksdorf, C. Birkner, A. Tejada, and N. Van De Wouw, "Fast Collision Probability Estimation for Automated Driving using Multi-circular Shape Approximations," in *2024 IEEE Intelligent Vehicles Symposium (IV)*. IEEE, 2024, pp. 2529–2536.

[33] A. Philipp and D. Goehring, "Analytic Collision Risk Calculation for Autonomous Vehicle Navigation," in *2019 International Conference on Robotics and Automation (ICRA)*. IEEE, 2019, pp. 1744–1750.

[34] M. Schreiner, *Bayesian Environment Representation, Prediction, and Criticality Assessment for Driver Assistance Systems*, 1st ed., ser. Verkehrstechnik/Fahrzeugtechnik. VDI Verlag, 2016, no. 797.

[35] J. Jansson and F. Gustafsson, "A framework and automotive application of collision avoidance decision making," *Automatica*, vol. 44, pp. 2347–2351, 2008.

[36] M. Kaufeld, M. Piccinini, and J. Betz, "MP-RBFN: Learning-based vehicle motion primitives using radial basis function networks," 2025.

[37] R. Wein, "2D Minkowski sums," in *CGAL User and Reference Manual*. CGAL Editorial Board, 2010, http //www.cgal.org.

[38] A. Kessy, A. Lewin, and K. Strimmer, "Optimal whitening and decorrelation," *The American Statistician*, vol. 72, p. 309–314, Jan. 2018.